Applied Surface Science 540 (2021) 148223

Contents lists available at ScienceDirect

Applied Surface Science

journal homepage: www.elsevier.com/locate/apsusc

Full Length Article

Potential energy surfaces of adsorption and migration of transition metal atoms on nanoporus materials: The case of nanoporus bigraphene and g-C_3N_4

Iuliia Melchakova[a], Kristina M. Nikolaeva[b], Evgenia A. Kovaleva[c], Felix N. Tomilin[b,c,d], Sergey G. Ovchinnikov[b,d], Olga N. Tchaikovskaya[c], Pavel V. Avramov[a,*], Alexander A. Kuzubov[b,1]

[a] Kyungpook National University, 80 Daehakro, Bukgu, Daegu 41566, Korea
[b] Siberian Federal University, 79 Svobodny Pr., Krasnoyarsk 660041, Russia
[c] Tomsk State University, 36 Lenin Ave., Tomsk 634050, Russia
[d] Kirensky Institute of Physics, FRC KSC SB RAS, 50 Akademgorodok, Krasnoyarsk 660036, Russia

ARTICLE INFO

The authors dedicate this article to the memory of Prof. Alexander A. Kuzubov.

Keywords:
Bigraphene
g-C_3N_4
Transition metal
Adsorption
Migration

ABSTRACT

First-row transition metal (TM) atoms adsorption and migration on nanoporus 2D materials like bigraphene with double vacancies and g-C_3N_4 as the active sites for TM nanocluster's growth was studied within the framework of density functional theory. Both thermodynamic and kinetic aspects of composite synthesis were discussed. It was found that potential barriers of adatom's migration from bigraphene's outer surface to the interlayer space through the double vacancy are rather low values. High potential barriers of TM migration along the carbon plane prevents TM clusterization due to enhanced chemical activity of double vacancies which gives a possibility to capture the surface adatoms. As was shown for the monolayer graphene, the decrease of vacancies concentration reduces the barrier of adatom migration along the surface while the second graphene sheet in bigraphene stabilizes the structure. The behavior of TM-atom regarding g-CN_2 and g-CN_1 nanosheets was investigated. Potential energy surfaces were obtained and discussed. The migration barriers were found surmountable that means high probability of migration of TM adatoms to global minima and formation of TM vacancies. Comparison of barriers values with Boltzmann factor demonstrated that just standalone temperature fluctuations cannot initiate structural transitions. The properties of designed structures can be of interest of catalysts and biosensors for biomedical applications.

1. Introduction

Graphene is known to be one of the most promising nanomaterials. Being one-atom-thick, it can be used in various electrochemical and photovoltaic applications, e.g. fuel cells or solar cells etc. [1]. Besides that, graphene possesses incredible conductivity and high surface area.

A number of experimental [1] theoretical [2–4] works are devoted to the investigation of the impurity effects on graphene's electronic structure and spin properties. Transition metal (TM) atoms which can be effectively adsorbed on graphene, have strong binding energy and can be applied for the substrate-based graphene systems [5]. Transition metal (TM) atoms primarily form covalent bonds with graphene atoms via strong hybridization between the adatom *d* orbitals and the *sp* orbitals of the graphene substrate, and charge transfer to graphene [6], particularly with atoms adsorbed on its vacancy sites [1,7,8]. The presence of vacancies increases the reactivity of carbon structure and allows sorprion of adatoms on graphene sheet. Transition metal atoms form covalent bonds with carbon atoms in the vicinity of the vacancies [9].

In order to estimate the lability of these structures, one has to know the height of potential barriers for TM adatoms migration along the surface. According to the results obtained by Krasheninnikov et al. [10], a perfect graphene sheet doesn't tend to form strong bonds with metal atoms. For instance, first-row transition metals like Ti, Co, Fe, Cr and Mn demonstrate energies of bonding with graphene surface lying in the range of (−0.2–1.5 eV). Along with that, the height of migration potential barriers (0.2–0.8 eV) witness a high movability of metal adatoms deposited on carbon surface.

* Corresponding author.
E-mail address: paul.veniaminovich@knu.ac.kr (P.V. Avramov).
[1] Deceased 12/31/2016.

https://doi.org/10.1016/j.apsusc.2020.148223
Received 10 August 2020; Received in revised form 5 October 2020; Accepted 18 October 2020
Available online 29 October 2020

Since vacancies are considered as the most favorable sites for metal atoms adsorption, one may be interested if vacancy-adsorbed atoms can leave the initial adsorption sites as easy as atoms adsorbed on perfect graphene sheet. Migration barriers calculated for single vacancy-adsorbed Au, Pt, Fe, Co and Ni were found to be relatively high and equal to 2.1, 3.1, 3.6, 3.2 and 3.1 eV, respectively [10], in a good agreement with experimental data (2.4 and 2.6 for Au and Pt, respectively) [9]. One could expect migration barriers of the same magnitude for other transition metal atoms as well.

Migration barrier calculated for Au atom adsorbed on the graphene double vacancy (5 eV) [10] also agrees well with experimental values [11]. Thus, in contrast to the ones adsorbed on a perfect graphene sheet, vacancy-adsorbed TM atoms are not likely to move along the surface at room temperature.

Previous study [12] demonstrated a possibility of TM atoms (TM = Cr, Fe, Mn, Ti and V) to be adsorbed on the outer surface of bigraphene and enter the interlayer space through the single vacancy. Height of calculated potential barriers between these two possible adsorption sites implies that such migration may occur at temperatures above 1000 K. This model can be used to describe the TM clusters formation on graphite thin flakes.

Double vacancies can be formed by migration and recombination of single vacancies at 3000 K [13]. Molecular dynamics simulations of vacancy behavior in graphene demonstrated [14] that the double vacancy is basically the 5–8-5 defect consisting of two pentagons and one octagon between them. Such 5–8-5 vacancy is extremely stable and doesn't undergo any structural changes up to 90 ps at 3000 K. It can be further transformed to 555–777 defect (three pentagons and three heptagons) by increasing temperature up to 3800 K [15].

A graphitic carbon nitride (g-C_3N_4), being structurally analogous to defected grapheme [16] and recently predicted to possess challenging electronic properties [17], now gains significant attention as a promising material for various applications in electronic devices [18–22]. There are two polymorphs of g-C_3N_4, namely, g-CN_1 constructed from triazine and g-CN_2 constructed from tri-s-triazine (heptazine) monomers, respectively [23]. Unlike most organic compounds, g-C_3N_4 is chemically and thermally stable [18,24–26]. It's water insoluble and can be synthesized using different techniques like CVD, PVD, solvothermal method etc [27]. The valence band of g-C_3N_4 is formed by the lone electron pair of nitrogen and π-bonding system so it could be tuned by changing chemical environment. Recently, g–C_3N_4 nanosheets doped by metal ions have been synthesized and catalytic efficiency of such nanostructures was examined [28]. It was found that catalytic efficiency could be ascribed to the band gap reduction, decrement of charge carrier recombination and the peroxymonosulfate (PMS) activation. Unfortunately, no attention was paid to the process of doping and migration barriers estimation [29,30].

This paper is aimed to describe the features of the first-row transition metal atoms adsorption and migration on bigraphene with double vacancy and g-C_3N_4 as the models for experimentally observed conditions of TM nanocluster's growth. Metallic clusters formation opens opportunities of using such material in catalysis and medicine as biosensor. This fact determines the importance of shading the light on the features of cluster formation. The results for bigraphene double vacancy are also compared with those for the bigraphene's single vacancy and graphene monolayer. To determine the role of bigraphene's second graphene layer in TM migration, structure calculations for TM migration through the single vacancy in single graphene layer.

2. Computational methods

All calculations were performed using Vienna Ab-initio Simulation Package (VASP) [31–33] within the DFT framework [34,35]. Plane wave basis set with projector augmented wave (PAW) method [36,37], GGA-PBE functional and Grimme correction for van-der-Waals interaction [38] were implemented. Single point calculations for bond nature analysis was made at GGA/PBE0 level of theory. Nudged elastic band (NEB) method was used for minimum energy path calculation of TM atom migration from outer surface to the inner space [39]. Monkhorst-Pack Brillouin zone k-point sampling was implemented, and the k-point mesh contained 12 × 12 × 1 k-points along *a*, *b* and *c* directions for the bigraphene and g-C_3N_4 unit cells, and 3 × 3 × 1 k-points for the corresponding supercells, respectively. A vacuum interval of 20 Å was set normal to the plane to avoid artificial interactions between adjacent images. The cutoff energy was equal to 400 eV. Maximum force acting on atoms being less than 0.001 eV/Å was used as a stopping criterion for structural optimizations.

The unit cell optimization was performed first for defectless bigraphene hexagonal cell (a = b = 2.45 Å, c = 20.00 Å) and then for bigraphene sheet with a double vacancy using 5 × 5 × 1 supercell. For further calculations of the migration barriers through the double vacancy the 3d metal atoms Mn and Ti were chosen. Since Mn and Ti atoms possess the smallest (2.94 and 3.78 eV, respectively) and the largest (5.82 and 6.60 eV, respectively) values of the migration barriers through the single vacancy amongst other 3d metal atoms [12] (see Section 3.2 for notations), they were considered in the study. Both outer surface and interlayer space were considered in order to estimate the migration barriers between two adsorption sites. The electronic structure calculations for TM migration through the monovacancy in single graphene layer were performed in order to shed the light on the role of bigraphene's second graphene layer in TM migration. In order to estimate the effect of concentration of the vacancies on the barrier height, two different supercells were considered: The first one had the same size as for bigraphene (5 × 5 × 1), and the second was four times bigger (10 × 10 × 1).

Two different isomers were considered for structural optimization of C_3N_4: g-CN_1 based on triazine and g-CN_2 based on heptazine (g-CN_x) [23]. TM/g-CN_1 and TM/g-CN_2 hybrid structures were then designed by filing each single vacancy of g-CN_1 and g-CN_2 with transition metal atom (TM = Mn, Fe) exactly inside the pore (plane) or atop the pore (out-of-plane). Two additional positions, namely, TM-ion atop the aromatic ring of CN_1 sheet (aromatic) and TM-ion placed in asymmetric position (asymmetric) (were also introduced) in order to describe the migration pathway along the surface (see Fig. 10).

3. Results and discussion

3.1. Model structures for TM adsorption

The unit cell optimization was performed for defectless bigraphene hexagonal cell (a = b = 2.45 Å, c = 20.00 Å) as well as for bigraphene sheet with a double vacancy using 5 × 5 × 1 supercell. Fig. 1 illustrates the optimized structure of double vacancy introduced in one graphene layer of bigraphene supercell. The 5-8-5 defect was formed during the geometry optimization process.

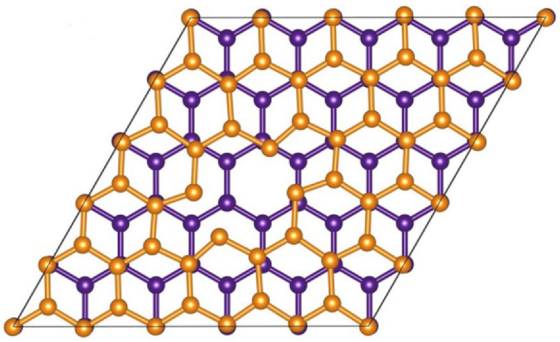

Fig. 1. Bigraphene with double vacancy after optimization, 5-8-5 defect is formed. Carbon atoms of upper and lower graphene layers are denoted as orange and purple balls, respectively.

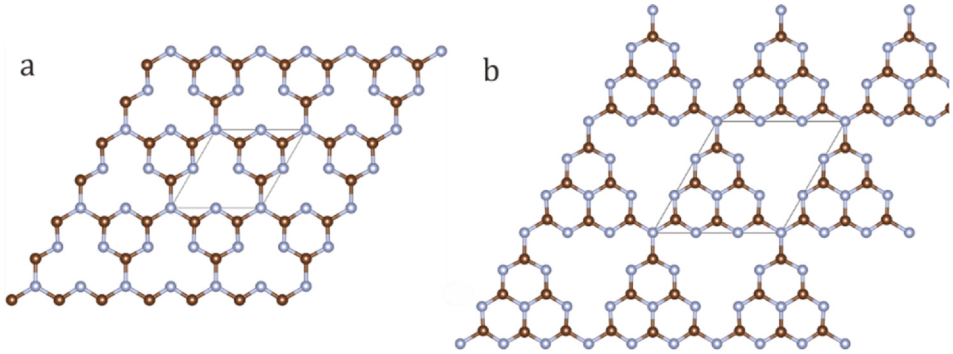

Fig. 2. Atomic structure of (a) g-CN_1 and (b) g-CN_2. The unit cells are indicated by the parallelograms. Carbon atoms are depicted in brown and nitrogen atoms are depicted in grey.

Table 1
Structural parameters of g-CN_1 and g-CN_2.

	a, Å (GGA/PBE)	a, Å (experiment)
g-CN_1	4.789	4.742
g-CN_2	7.102	7.113

Fig. 2 demonstrates the results of free-standing g-CN_1 and g-CN_2 geometry optimization. Corresponding unit cell parameters are presented in Table 1 and display good agreement with experimental data [25]: the divergences with the experimental XRD data are equal to 1% for g-CN_1 and 0.15% for g-CN_2.

3.2. TM atoms adsorption on double vacancy in bigraphene

Since Mn and Ti atoms possess the smallest (2.94 and 3.78 eV, respectively) and the largest (5.82 and 6.60 eV, respectively) values of the migration barriers through the single vacancy amongst other 3d metal atoms [12] (see Section 3.2 for notations), they were chosen for further calculations. Binding energies and structural parameters of Mn and Ti atoms adsorbed on single and double vacancies in bigraphene are summarized in Table 2. Likewise the previous study [12], both outer surface and interlayer space were considered in order to estimate the migration barriers between two adsorption sites.

The Fig. 3 presents the 5 × 5 × 1 supercell of bigraphene ($a = b = 2.45$ Å, $c = 20.00$ Å) with single vacancy and adsorbed transition metal. It demonstrates structural features of the system under consideration. Here, D_1 is the distance between the transition metal and the nearest atomic carbon atom at the site of vacancies while indicates the distance between the transition metal and the carbon plane below the metal. Binding energies of TM atoms with bigraphene sheet notably decreased comparing to the case of single vacancy adsorption which can be attributed to larger metal to carbon atoms due to the size of double vacancy (see Table 2). When TM is adsorbed on the double vacancy from outside of the carbon surface, the metal is attracted closer than in the case of monovacancy due to the stronger binding of TM to the double vacancies. Therefore, the distance D_2 (the distance between the transitional metal and the pore) for monovacancies is almost twice as much as for double vacancies. On the contrary, when the metal is embedded into the vacancy, i.e. in the interlayer space, the metal atom moves away from the carbon surface. Hence, the distance D_2 for the interlayer space is larger than D_2 for bilayer graphene on the surface. This can be explained by the influence of the second layer of graphene which will attract TM, thereby increasing the distance.

Fig. 4 shows spatial spin density distribution in bigraphene with double vacancy filled by Mn adatom. Manganese atom demonstrates positive magnetic moment due to unpaired d-electrons, and four nearest carbon atoms gain negative spin polarization giving the net magnetic moment of 3 μ_B for both inner- and outer-sorbed Mn. No spin polarization was observed for Ti-based structure.

3.3. Migration pathways of TM atoms in the vicinity of double vacancy

Potential barriers of TM atoms migration through the double vacancy (see Fig. 5) are summarized in Table 3. As can be seen, TM atoms can move through the double vacancy much easier than through the single one [12]. For example, the Mn atom moves through a double vacancy from the surface to the interlayer space with a barrier of 0.38 eV in contrast to 2.94 eV barrier in case of single one vacancy. This can be attributed to the increased volume of the vacancy with respect to the surface area as well as the decreased binding energies with bigraphene surface: The higher the binding energy, the less the mobility of adsorbed atom. Migration equilibrium is shifted to formation of inner-sorbed complex for both Mn and Ti, in agreement with the data regarding single vacancy [11].

In order to estimate the stability of the TM/bigraphene complexes, the migration pathways of TM atoms out of the vacancy along the surface were simulated (Fig. 6). A TM atom can either go in or out of the vacancy by relocating between several sites schematically denoted in Fig. 6 as 1, 2, 3 and 4. The starting position for the metal atom is the center of the vacancy denoted as position 1. It then starts moving to the corner, e.g. position 2. Approaching position 3 or 4 requires leaving the vacancy and binding to the neighboring hexagons of the carbon surface.

Table 2
Binding energies and structural parameters for Ti and Mn atoms adsorbed on single and double bigraphene vacancies.

TM	Property	Double vacancy		Single vacancy	
		Inner sorption	Outer sorption	Inner sorption	Outer sorption
Ti	Binding energy, eV	−1.99	−1.17	−3.25 [12]	−2.61 [12]
	TM-C shortest distance (D_1), Å	2.09	2.05	2.01	1.98
	Distance to the carbon plane (D_2), Å	0.89	0.82	1.61	1.53
Mn	Binding energy, eV	−0.83	−0.47	−2.93 [12]	−2.18 [12]
	TM-C shortest distance (D_1), Å	1.99	1.97	1.83	1.80
	Distance to the carbon plane (D_2), Å	0.68	0.56	1.29	1.22

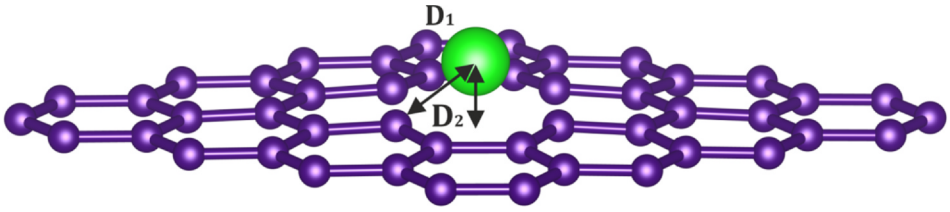

Fig. 3. Structural parameters of TM atom adsorption on bivacancy in bigraphene. TM and carbon atoms are denoted as gold and purple balls, respectively. D_1 is the distance between the transition metal and the nearest atomic carbon atom at the site of vacancies. D2 is the distance between the transitional metal and the pore.

The results of potential energy surface scanning performed by applying NEB method to each transition are presented in Table 4.

The transition of metal atom from position 1, to position 2 has the maximum height of potential barrier both for monovacancy and double vacancy (Table 3). The more TM-carbon bonds are formed, the more stable the structure is. When moving to the position 2, TM atom loses one bond with carbon while others deform and become weaker. However, 1–2 transition has lower barrier for double vacancy than for the single one (Table 4). This fact may be explained in terms of structure stabilization via forming 5-8-5 defect with TM atom inside which is not possible when large TM atom adopts the position 1 (Fig. 7). Fig. 7 shows the change in the length of C–C bonds due to the migration of the transition metal atom along the surface.

Next, the TM atom can move to either position 3 or 4 (2–3 and 2–4 transitions in Fig. 6b). For both pathways the potential barriers are lower than the 1–2 one but still considerably high (Table 4). In contrast, inverse barriers for transitions of metal atoms back to the center of the vacancy are much lower than direct barriers witnessing the stability of initial structures. For example, the barrier of Mn transition from position 1 to position 2 is 4.22 eV while the inverse transition from position 2 to position 1 is only 0.02 eV (Table 4).

Probability of Mn migration at double vacancy was evaluated using equilibrium constants (Table 5), calculated as the ratio of corresponding rate constants using the Arrhenius equation:

$$K = \frac{k_{approach}}{k_{removal}} = \frac{e^{\frac{-E_{barrier}r_{approach}}{kT}}}{e^{\frac{-E_{barrier}r_{removal}}{kT}}} \quad (1)$$

Here A (pre-exponential) factors were omitted, T is temperature, $E_{barrier}$ is the height of the potential barriers, which were defined as the difference in energies between the top of the potential barrier and the minimum at the potential energy curves.

The values of the equilibrium constants at a temperature of 298 K are very low, the migration outside the vacancy of Mn is very unlikely. This indicates the stability of the initial structures.

3.3.1. TM migration outside the vacancy in single graphene layer

Electronic structure calculations for TM migration pathways through the monovacancy in single graphene were performed in order to shed light on the role of bigraphene second graphene layer in TM migration on top of bigraphene. In order to estimate the effect of concentration of the vacancies on the barrier, two different supercells were considered: The first one was the same as for bigraphene sheet (5 × 5 × 1), and the second was four times bigger (10 × 10 × 1).

The Fig. 8 shows the Mn atom passing through the mono-vacancy by approaching the carbon lattice, entering the vacancy and exiting from it on the other side of graphene sheet. Table 6 shows the results of potential barrier calculations.

10 × 10 × 1 supercell demonstrates 21% lower barrier for migration of Mn than 5 × 5 × 1 one does, and 13% barrier decreasing is observed for Ti. Thus, the less the vacancy concentration, the less additional tension of the whole structure is, lowering the migration barrier. Values of migration barriers for monolayer graphene are actually in between of those for the outer-inner transition and the inner-outer one (see Table 6). For example, the value of the migration barrier for the Mn atom in a single layered graphene is 3.14 eV, which is an intermediate value between the transition to the outer surface of 3.78 eV and the interlayer space of 2.94 eV. The second layer in bigraphene does stabilize the adsorbed TM atom by increasing the inner-outer barrier and decreasing the outer-inner one. This is confirmed by the values of binding energies of TM atoms with single layered graphene (see Table 7) which are also in between of corresponding inner and outer sorption energies.

3.3.2. Adsorption of Fe and Mn atoms by g-C_3N_4

To localize global and local minima in TM/C_3N_4 hybrid structures (TM = Fe, Mn), several possible coordinations of TM atoms were considered. Structural optimizations reveal 4 energy minima, namely plane site (denoted as a,c, Fig. 9) with TM-atoms coordinated to the center of the vacancies in g-CN_x matrix and out-of-plane site (denoted as b,d in Fig. 9) with TM atoms coordinated above the vacancies.

The energy differences between planar and out-of-plane conformers

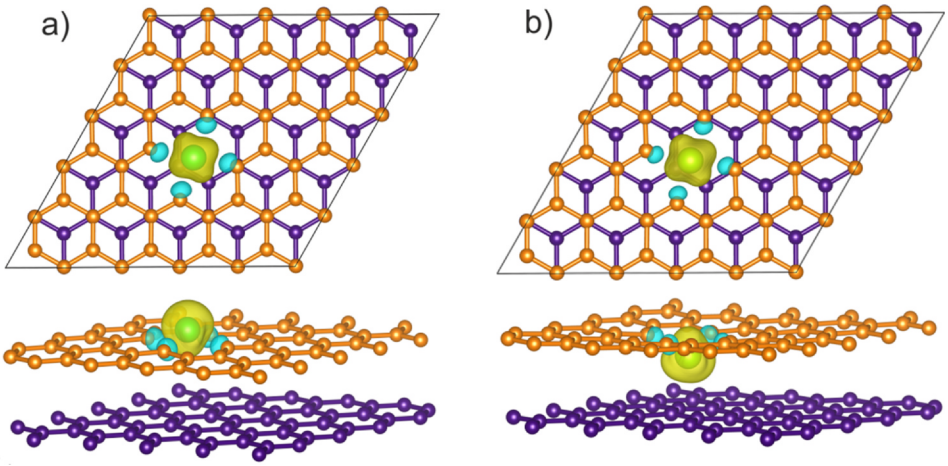

Fig. 4. Spin density spatial distribution in (a) outer-sorbed Mn; (b) inner-sorbed Mn on bigraphene's double vacancy. Carbon atoms of upper and lower graphene layers are denoted as orange and purple balls. Yellow (blue) areas correspond to spin-up (spin-down) density.

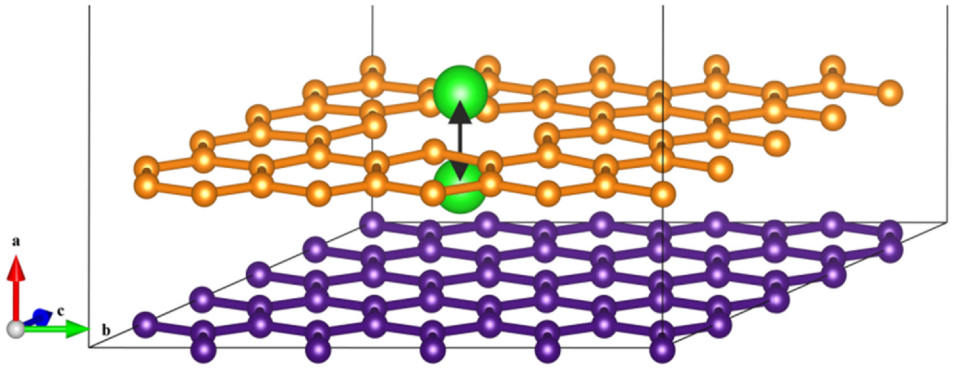

Fig. 5. The transition metal migrates from the surface of bilayer graphene, passing through a bivacancy into the interlayer space. TM and carbon atoms are denoted as gold and purple balls, respectively. Bigraphene's second layer is not presented for the sake of better representation.

Table 3
Potential barriers of TM atom migration from the outer surface of bigraphene to its interlayer space and vice versa through the single and double vacancies.

TM	Height of migration barrier, eV			
	Double vacancy		Single vacancy	
	To the interlayer space	To the outer surface	To the interlayer space	To the outer surface
Ti	2.15	2.97	5.82 [12]	6.60 [12]
Mn	0.38	0.74	2.94 [12]	3.78 [12]

were calculated using the formula:

$$\Delta E = E_{plane} - - E_{out-of-plane}, \quad (2)$$

where E_{plane} and $E_{out\text{-}of\text{-}plane}$ stand for the total energies of the plane and out-of-plane structures, respectively. It was estimated that out-of-plane conformer is energetically favorable in comparison with planar one (Table 8).

Calculated structural parameters of TM/g-CN_1 and TM/g-CN_2 conformers are presented in Table 8. The structure calculations revealed that the unit cell parameters of TM/g-CN_1 depend upon the ionic radii of TM atoms, whereas the structure of TM/g-CN_2 remains unchanged because of relatively large vacancies of pristine g-CN_2.

The electronic structure calculations revealed low-spin state (3.10μ_B, 2.00μ_B, 4.96 μ_B, and 3.74 μ_B) to be favorable for TM/g-CN_1 and high-spin state (4.58μ_B, 3.33μ_B, 4.80μ_B, 3.71μ_B) to be favorable for TM/g-CN_2 hybrid structures, respectively. Also the differences between magnetic moments (Table 8) for planar and out-of-the-plane TM/g-CN_1 can define the changes of electron transport and the bonding nature of TM ion with nitrogen sites. Low-spin states can be realized by an electron transfer of nitrogen lone electron pair to vacant d-orbitals of Fe/Mn atoms. This assumption could be proved by the Fig. 10 showing how the positive spin density localizes at both TM and nitrogen sites indicating direct chemical interactions between them. The short

Table 4
Potential barriers for TM atom migration pathways on defect mono- and bigraphene (Fig. 6).

Metal	Migration step	Height of migration barrier, eV			
		Double vacancy		Monovacancy	
		Direct	Inverse	Direct	Inverse
Mn	1–2	4.22	0.02	5.25	0.03
	2–3	1.51	0.13	1.12	0.32
	2–4	–	–	0.92	0.43
Ti	1–2	3.56	0.03	5.00	0.01
	2–3	1.47	0.09	0.86	0.29
	2–4	–	–	0.70	0.52

distances between nitrogen and TM atoms lead to electron transfer from p-orbitals of nitrogen to d-orbitals of TM. Contrary to previously mentioned, out-of-the-plane structure spin density is much more localized at TM ion (Figs. 10 and 11).

TM-atom – nitrogen chemical bonding for both Fe and Mn was found to be that strong that there is no way to keep metal atom n the surface of TM/g-CN_2 heterostructure, i.e. TM-atoms should penetrate inside the pore. In contrast to that, small size of the g-CN_1 vacancy keeps both TM-atoms out of the pore.

3.3.3. Migration of Fe and Mn atoms on g-C_3N_4 lattices

The little chance due to high potential energy barrier of TM-atom penetration into the g-CN_1 pore along with g-CN_1 structure shape allows one to assume a presence of different metal configurations at TM/g-CN_1 surface. In addition to two adsorption sites studied before, another two points on potential energy surfaces were considered to investigate the migration pathways of Fe and Mn atoms on g-CN_1. Thus, four different positions of TM-ion were considered, namely, aromatic (1), asymmetric (2), out-of-the-plane (3) and plane (4) sites (Fig. 12). Different migration pathways were chosen to estimate the barriers and

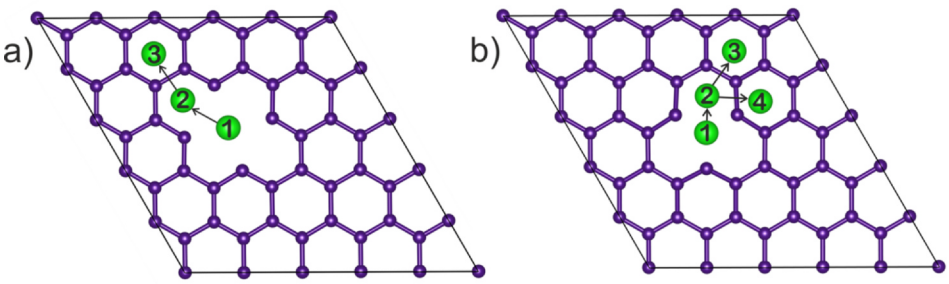

Fig. 6. Model for the TM migration path out of the (a) double vacancy; (b) single vacancy. TM and carbon atoms are denoted as green and purple balls, respectively.

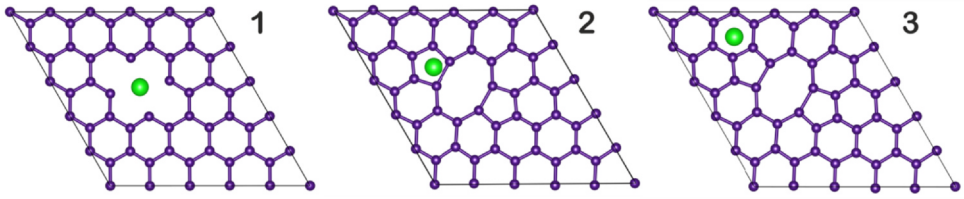

Fig. 7. Structural changes (from left to right) of the vacancy during the migration of a metal atom over a surface: bonds deformation and formation of a 5-8-5 defect. Carbon atoms are depicted in Violet; TM atom is depicted in light green.

Table 5
Equilibrium constants for Mn migration at double vacancy.

Migration step	Equilibrium constants	
	Double vacancy K, k_1/k_2	Monovacancy K, k_1/k_2
1–2	$4{,}55 \cdot 10^{-68}$	$4{,}76 \cdot 10^{-90}$
2–3	$1{,}76 \cdot 10^{-28}$	$3{,}27 \cdot 10^{-14}$

Table 6
Potential barriers for TM migration through the monovacancy in single graphene layer.

Supercell size	TM	Height of migration barrier, eV		
		Single layered graphene	Bigraphene	
			To the interlayer space	To the outer surface
5 × 5 × 1	Mn	3.14	2.94	3.78
10 × 10 × 1		2.47	–	–
5 × 5 × 1	Ti	6.20	5.82	6.60
10 × 10 × 1		5.40	–	–

Table 7
Binding energies for TM atoms adsorbed on bilayered graphene.

Supercell size	TM	Binding energy, eV		
		Single layered graphene	Bigraphene	
			Inner sorption	Outer sorption
5 × 5 × 1	Mn	−2.22	−2.93	−2.18
10 × 10 × 1		−1.40	–	–
5 × 5 × 1	Ti	−3.24	−3.25	−2.61
10 × 10 × 1		−1.65	–	–

assume the probability of transitions between the sites.

A global minimum for TM/g-CN_1 was localized during the procedure of barrier calculations. Asymmetric (2) position was eventually found to be energetically favorable with energy difference of −0.67 eV in comparison with out-of-plane (3) position. The reason of total energy decreasing is supposed to be relaxation and little distortion from plane nanosheet, i.e. deviation from initial planar shape.

The NEB method was used to calculate barriers along 1-2-3-4 migration pathways (Table 9). Minimal energy path for TM-CN_1 is presented in Fig. 13. It was found that the Fe atom coordinates only to asymmetric (2) position, while Mn coordinates both to aromatic (1) and asymmetric (2) positions because of relatively high transition barrier presence 1(1.91 eV). Due to high values of inverse (2 → 3 and 3 → 4) barriers (2.65 eV, 4.18 eV) it can be estimated a little probability of such inverse transition. Comparison of the data with temperature factor demonstrate that metal atoms will form metallic clusters, i.e. the least value is 0.34 eV that corresponds to 3945 K and the temperature fluctuation cannot initiate the migration. It means that all Fe atoms wherever they are initially placed should migrate to asymmetric (2) positions, while all Mn atoms should migrate to either aromatic (1) or asymmetric (2) positions

4. Bond nature analysis

To analyze the nature of chemical bonding, orbital resolved of Np-, Cp-, and Fe/Mnd-states partial density of states (PDOSes) were calculated at GGA/PBE0 level of theory (Fig. 14). Alongside 4 above-mentioned localized structural minima, all transition states were examined as well. The analysis demonstrates similar results for Fe/g-CN_1 and Mn/g-CN_1. The characterization of TM/g-CN_1 heterostructure electronic properties is presented in Fig. 14.

TM/g-CN_1 (TM = Mn, Fe) heterostructures (Fig. 14) can be defined as a medium band gap semiconductors for both α and β spin channels (1.1 eV and 1.6 eV band gaps for Mn/g-CN_1 and Fe/g-CN_1, respectively). The structures can be characterized as highly spin-polarized due to high asymmetry of DOS intensities at different spin channels. In β spin channel, the 1 and 5 peaks coincidence demonstrates mixture of Np_z orbitals with Cp_z and $Mnd_{x^2-y^2}$ due to a good

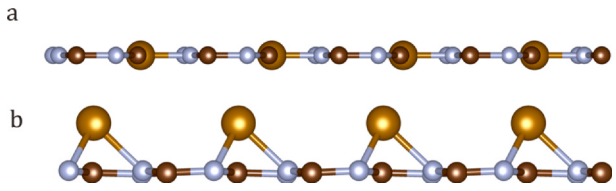

Fig. 9. Atomic structure of planar (a,c) Fe/g-CN_x and out-of-plane (b,d) Fe/g-CN_x for g-CN_1 (top) and g-CN_2 (bottom). The Fe atoms are depicted in golden, the carbon and nitrogen atoms are depicted in grey and brown, respectively. Mn/g-CN_x heterostructures have the same crystalline lattices but different lattice constants listed in Table 8.

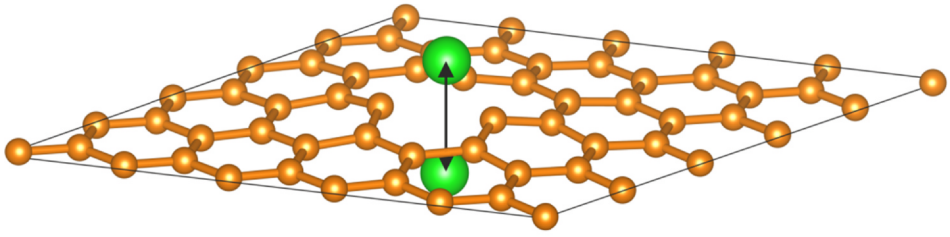

Fig. 8. TM migration pathway through the monovacancy in single-layer graphene (5 × 5 × 1). Carbon atoms are depicted in yellow, TM atom is depicted in light green. The arrow indicates the direction of sorption.

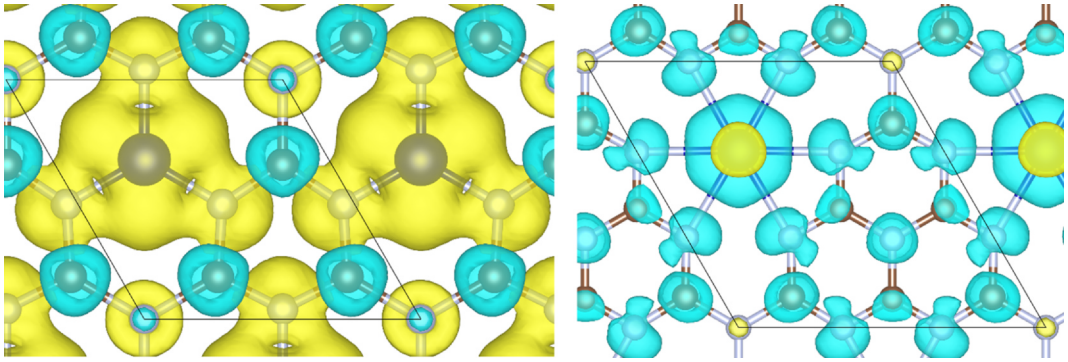

Fig. 10. Spatial distribution of spin density of plane Mn/g-CN_1 (a) and Mn/g-CN_2 (b). Spin-down spin-density is depicted in blue and spin-up spin density is depicted in yellow. The unit cells are indicated by parallelograms. The carbon atoms are depicted in brown and nitrogen atoms are depicted in grey, the Mn atoms are depicted in purple.

Table 8
Lattice parameters (a, Å), metal-nitrogen bond lengths (Me-N, Å), magnetic moments (μ, μ_B) and energy difference (ΔE, eV) of TM/g-CN_1 and TM/g-CN_2 hybrid compounds.

TM ion	Planar			Out-of-plane			ΔE, eV
	a, A	Me-N, Å	Magnetic moment, μ_B	a, A	Me-N, Å	Magnetic moment, μ_B	
TM/g-CN_1							
Mn	5.39	1.71	3.10	4.83	2.05	4.58	−2.963
Fe	5.23	1.79	2.00	4.83	1.97	3.33	−2.033
TM/g-CN_2							
Mn	7.10	2.35	4.96	7.05	2.35	4.80	−0.257
Fe	7.10	2.35	3.74	7.05	2.35	3.71	−0.220

match of the PDOSes shapes in [−2;0] eV energy interval. α spin channel demonstrates Mn$d_{x^2-y^2}$, Mn d_{xz}, Np_z, and Cp_z mixture in [−3; 0] eV energy interval (peaks number 2–4) as well as Np_z, Mn d_{xz},Mn$d_{x^2-y^2}$ mixture in [1.3; 3] eV energy range for vacant states. The orbital mixing analysis for Fe/g-CN_1 demonstrates the mixture of Np_z orbitals with Fe d_{xy} and Fe $d_{x^2-y^2}$ due to a good match in α spin channel [−3;0] eV energy range (peaks number 3–4). β spin state Fe d_{xy}, Fe $d_{x^2-y^2}$, Np_z, Cp_z, mixture in [−1.7; 0] eV (peaks number 1 and 5). In sum up, the Fe/g-CN_1 clearly demonstrates complex bonding between Fe atoms and g-C_3N_4 in contrast with Mn/g-CN_1 for which the Mn atoms are bonded to g-C_3N_4 by simple Coulomb interactions.

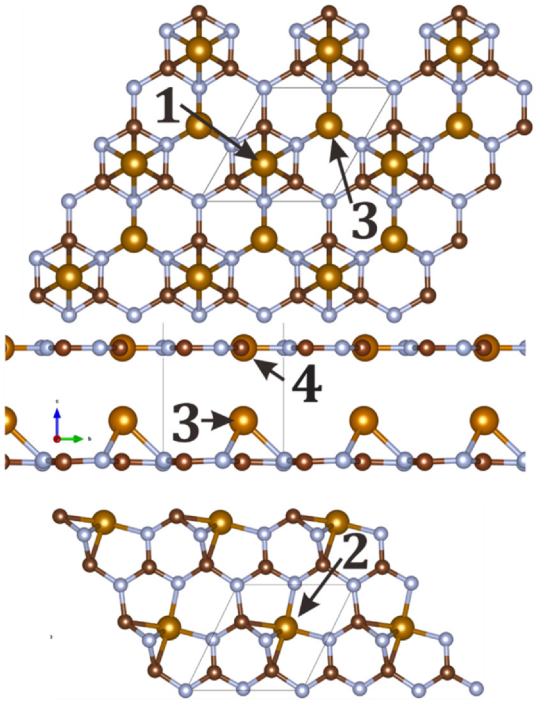

Fig. 12. Sites of TM atoms on g-CN_1. The unit cells are indicated by parallelograms. The Fe/Mn atoms are depicted in golden. Each single position is indicated by correspondent numbers: aromatic (1), asymmetric (2), out-of-the-plane (3) and plane (4).

5. Conclusions

The pathways of TM atoms (Ti, Mn, Fe) adsorption and migration at 2D g-CN_x and double-vacancy bigraphene sheets were investigated using state-of-the-art GGA PW PBC electronic structure calculations. First-row transition metal atoms adsorption on bigraphene double vacancy is characterized by lower binding energies and potential barriers of migration between inner and outer adsorption sites in comparison with those of single-vacancy bigraphene. The comparison of the absorption energies revealed that formation of inner-sorbed complexes is preferable, and potential barriers of TM atoms migration along the

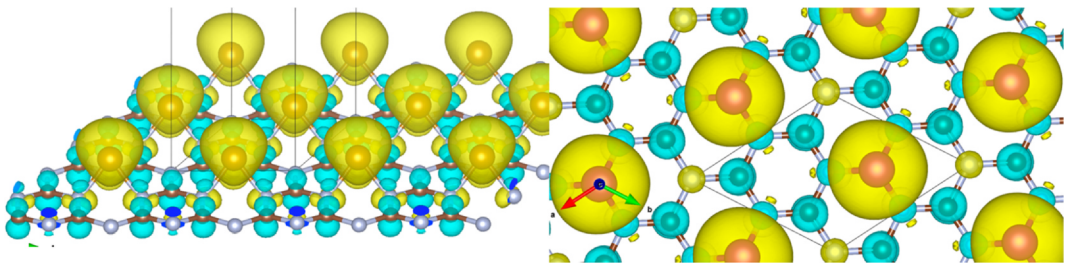

Fig. 11. Spatial distribution of spin density of out-of-plane Fe/g-CN_1 from different sides (left/right). The negative spin-density is depicted in blue and the positive spin density is depicted in yellow. The unit cells are indicated by parallelograms. The carbon atoms are depicted in brown and nitrogen atoms are depicted in grey, the Fe ions are depicted in gold.

Table 9
Potential barriers (eV) for TM atom migration in g-CN_1.

Metal	1 → 2		2 → 3		3 → 4	
	Direct	Inverse	Direct	Inverse	Direct	Inverse
Mn	1.91	0.34	1.22	4.18	3.29	0.43
Fe	0.44	2.65	1.59	0.44	2.40	0.37

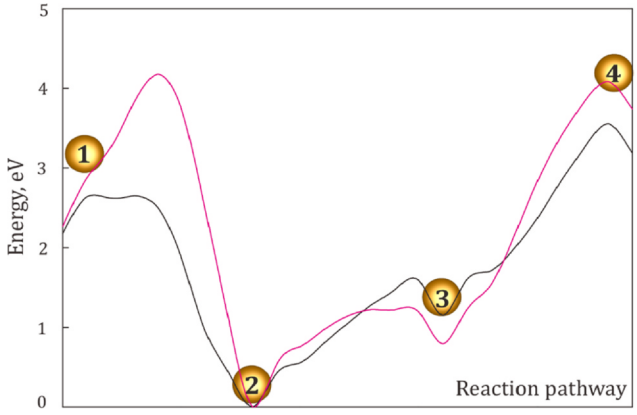

Fig. 13. Minimum energy paths of Fe and Mn atoms migration in g-CN1, depicted in black and purple, respectively. Each position is indicated by correspondent number in golden circle (Fig. 10).

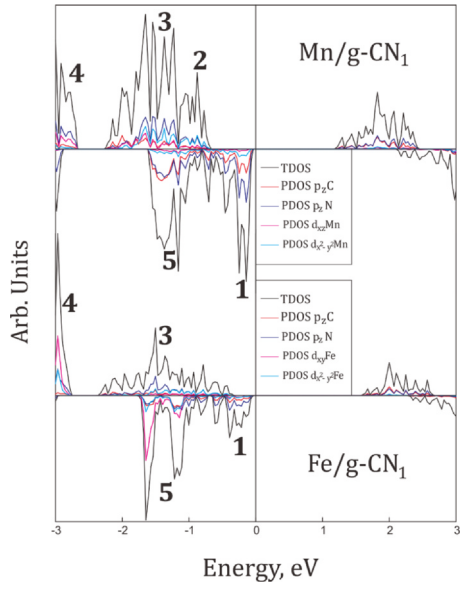

Fig. 14. Orbital resolved GGA/PBE0 PDOSes of Mn/g-CN_1 heterostructure global minimum (2 – Asymmetric position) (top) and PDOS of Fe/g-CN_1 heterostructure global minimum (2 – Asymmetric position) (bottom).

surface outside vacancy are considerably high ensuring the stability of the hybrid structures. Bigraphene's second layer was proved to play an important role in stabilization of the structures due to the formation of inner-sorbed complexes. Fe/Mn atoms was found to penetrate g-CN_2 nanosheet, while at g-CN_1 they stay at the surface. The transition state of Fe site was estimated at 7.5 Å distance from g-CN_1. It was found that asymmetric (2) position is energetically favorable and the Fe atom can migrate to it from aromatic (1) and out-of-plane (3) sites. It was found as well that metal atoms can form metallic clusters. The unique atomic and electronic structure and spin properties of nanoporus 2D TM/bigraphene and TM/g-C_3N_4 heterostructures is very promising for advanced applications as catalysts and biosensors for biomedical applications.

CRediT authorship contribution statement

Iuliia Melchakova: Writing - original draft, Writing - review & editing, Visualization, Data curation. **Kristina M. Nikolaeva:** Writing - original draft, Writing - review & editing, Visualization, Data curation. **Evgenia A. Kovaleva:** Conceptualization, Validation, Data curation. **Felix N. Tomilin:** Conceptualization, Resources. **Sergey G. Ovchinnikov:** Project administration. **Olga N. Tchaikovskaya:** Project administration. **Pavel V. Avramov:** Conceptualization, Validation, Project administration, Supervision. **Alexander A. Kuzubov:** Conceptualization.

Declaration of Competing Interest

The authors declare that they have no known competing financial interests or personal relationships that could have appeared to influence the work reported in this paper.

Acknowledgements

The authors would like to thank Joint Supercomputer Center of RAS, Moscow; Center of Equipment for Joint Use of Siberian Federal University, Krasnoyarsk; and Information Technology Centre, Novosibirsk State University for providing the access to their supercomputers. Publication was supported by Project FSWM-2020-0033 of Russian Ministry of Science and Education.

References

[1] O. Cretu, A.V. Krasheninnikov, J.A. Rodríguez-Manzo, L. Sun, R.M. Nieminen, F. Banhart, Phys. Rev. Lett. 105 (2010) 196102.
[2] E.J.G. Santos, A. Ayuela, S.B. Fagan, J. Mendes Filho, D.L. Azevedo, A.G. Souza Filho, D. Sánchez-Portal, Phys. Rev. B - Condens. Matter Mater. Phys. 78 (2008) 195420.
[3] S. Ejg, A. Ayuela, D. Sánchez-Portal, New J. Phys. 12 (2010) 053012.
[4] P.Y. Xie, G.L. Zhuang, Y.A. Lü, J.G. Wang, X.N. Li, Wuli Huaxue Xuebao/Acta Phys. - Chim. Sin. 28 (2012) 331–337.
[5] Y. Mao, J. Yuan and J. Zhong, J. Phys. Condens. Matter., DOI:10.1088/0953-8984/20/11/115209.
[6] N. Dimakis, F.A. Flor, A. Salgado, K. Adjibi, S. Vargas, J. Saenz, Appl. Surf. Sci. 421 (2017) 252–259.
[7] W. Zhang, L. Sun, Z. Xu, A.V. Krasheninnikov, P. Huai, Z. Zhu, F. Banhart, Phys. Rev. B - Condens. Matter Mater. Phys. 81 (2010) 125425.
[8] O.V. Yazyev, A. Pasquarello, Phys. Rev. Lett. 100 (2008) 156102.
[9] L. Hu, X. Hu, X. Wu, C. Du, Y. Dai, J. Deng, Phys. B Condens. Matter 405 (2010) 3337–3341.
[10] A.V. Krasheninnikov, P.O. Lehtinen, A.S. Foster, P. Pyykkö, R.M. Nieminen, Phys. Rev. Lett. 102 (2009) 126807.
[11] S. Malola, H. Häkkinen, P. Koskinen, Appl. Phys. Lett. 94 (2009) 043106.
[12] H. Sevinçli, M. Topsakal, E. Durgun, S. Ciraci, Phys. Rev. B - Condens. Matter Mater. Phys. 77 (2008) 195434.
[13] A.A. Kuzubov, P.V. Avramov, K.M. Nikolaeva, N.S. Mikhaleva, E.A. Kovaleva, A.V. Kuklin, A.S. Fedorov, Comput. Mater. Sci. 112 (2016) 269–275.
[14] W. Hong, H.N. Lee, M. Yoon, H.M. Christen, D.H. Lowndes, Z. Suo, Z. Zhang, Phys. Rev. Lett. 95 (2005) 095501.
[15] C.Z. Wang, G. Do Lee, J. Li, S. Yip, K.M. Ho, Sci. Model. Simul. SMNS 15 (2008) 97–121.
[16] Y. Wang, X. Wang, M. Antonietti, Angew. Chemie Int. Ed. 51 (2012) 68–89.
[17] A.Y. Liu, M.L. Cohen, Science (80-) 245 (1989) 841–842.
[18] J. Yang, X. Wu, X. Li, Y. Liu, M. Gao, X. Liu, L. Kong, S. Yang, Appl. Phys. A 105 (2011) 161–166.
[19] H. Yan, Y. Chen, S. Xu, Int. J. Hydrogen Energy 37 (2012) 125–133.
[20] J. Fu, B. Chang, Y. Tian, F. Xi, X. Dong, J. Mater. Chem. A 1 (2013) 3083.
[21] S.C. Yan, Z.S. Li, Z.G. Zou, Langmuir 26 (2010) 3894–3901.
[22] T. Tyborski, C. Merschjann, S. Orthmann, F. Yang, M.-C. Lux-Steiner, T. Schedel-Niedrig, J. Phys. Condens. Matter 24 (2012) 162201.
[23] G. Dong, Y. Zhang, Q. Pan, J. Qiu, J. Photochem. Photobiol. C Photochem. Rev. 20 (2014) 33–50.
[24] Y. Li, J. Zhang, Q. Wang, Y. Jin, D. Huang, Q. Cui, G. Zou, J. Phys. Chem. B 114 (2010) 9429–9434.
[25] S.C. Yan, Z.S. Li, Z.G. Zou, Langmuir 25 (2009) 10397–10401.
[26] E.G. Gillan*, , DOI:10.1021/CM000570Y.
[27] A. Thomas, A. Fischer, F. Goettmann, M. Antonietti, J.-O. Müller, R. Schlögl, J.M. Carlsson, J. Mater. Chem. 18 (2008) 4893.

[28] A. Durairaj, T. Sakthivel, A. Obadiah, S. Vasanthkumar, J. Mater. Sci. Mater. Electron. 29 (2018) 8201–8209.
[29] D. Ghosh, G. Periyasamy, B. Pandey, S.K. Pati, J. Mater. Chem. C 2 (2014) 7943–7951.
[30] Y. Zhang, Z. Wang, J. Cao, J. Mater. Chem. C 2 (2014) 8817–8821.
[31] G. Kresse, J. Hafner, Phys. Rev. B 47 (1993) 558–561.
[32] G. Kresse, J. Hafner, Phys. Rev. B 49 (1994) 14251–14269.
[33] G. Kresse, J. Furthmüller, Phys. Rev. B - Condens. Matter Mater. Phys. 54 (1996) 11169–11186.
[34] P. Hohenberg, W. Kohn, Phys. Rev. 136 (1964) B864.
[35] W. Kohn, L.J. Sham, Phys. Rev. 140 (1965) A1133.
[36] P.E. Blöchl, Phys. Rev. B 50 (1994) 17953–17979.
[37] G. Kresse, D. Joubert, Phys. Rev. B 59 (1999) 1758–1775.
[38] S. Grimme, J. Comput. Chem. 27 (2006) 1787–1799.
[39] G. Henkelman, B.P. Uberuaga, H. Jónsson, J. Chem. Phys. 113 (2000) 9901–9904.